Calibration and Experimental Studies on the Mixing Parameters of Red Clover Seeds and Coated Powders

Authors:

Xuejie Ma, Min Liu, Zhanfeng Hou, Junru Li, Xiangyu Gao, Yang Bai, Mengjun Guo

Date Submitted: 2023-02-21

Keywords: Computational Fluid Dynamics, EDEM, discrete element method, parameter calibration

Abstract:

The physical and mechanical properties of the materials in the swirling fluidized-bed seed pelleting unit affect the mixing degree of the materials in the pelleting and coating process, which is of great significance to research on pelleting and coating. The problem of discrete particle model parameters affecting CFD-DEM simulation results is addressed. In this paper, red clover seeds (referred to as seeds) and pelletized coating powder (referred to as powder) were used as the research objects, and the JKR. model was selected to calibrate the contact parameters between seeds and powder based on particle amplification theory. With the powder rest angle as the response value, a simulation calibration test was conducted; the parameters with significant effects on the response value were screened based on the Plackett?Burman test, and the steepest climb test determined the range of factor levels of essential parameters. The Box?Behnken test was used to establish the curvilinear response surface and quadratic regression equation to determine the best combination of simulation parameters for the powder. The discrete element rest angle was conducted with the best combination of parameters. The error of the test compared with the physical examination was 1%. The particles calibrated by simulation were subjected to the pneumatic suspension velocity test and particle mixing test. The test results matched the physical test results, which further verified the accuracy and applicability of the established discrete element model and parameters for coated powders.

Record Type: Published Article

Submitted To: LAPSE (Living Archive for Process Systems Engineering)

Citation (overall record, always the latest version):	LAPSE:2023.0806
Citation (this specific file, latest version):	LAPSE:2023.0806-1
Citation (this specific file, this version):	LAPSE:2023.0806-1v1

DOI of Published Version: https://doi.org/10.3390/pr10112280

processes

MDPI

Article

Calibration and Experimental Studies on the Mixing Parameters of Red Clover Seeds and Coated Powders

Xuejie Ma †, Min Liu †, Zhanfeng Hou *, Junru Li, Xiangyu Gao, Yang Bai and Mengjun Guo

College of Mechanical and Electrical Engineering, Inner Mongolia Agricultural University, Hohhot 010018, China
* Correspondence: njau-hzf@163.com
† These authors contributed equally to this work.

Abstract: The physical and mechanical properties of the materials in the swirling fluidized-bed seed pelleting unit affect the mixing degree of the materials in the pelleting and coating process, which is of great significance to research on pelleting and coating. The problem of discrete particle model parameters affecting CFD-DEM simulation results is addressed. In this paper, red clover seeds (referred to as seeds) and pelletized coating powder (referred to as powder) were used as the research objects, and the JKR. model was selected to calibrate the contact parameters between seeds and powder based on particle amplification theory. With the powder rest angle as the response value, a simulation calibration test was conducted; the parameters with significant effects on the response value were screened based on the Plackett–Burman test, and the steepest climb test determined the range of factor levels of essential parameters. The Box–Behnken test was used to establish the curvilinear response surface and quadratic regression equation to determine the best combination of simulation parameters for the powder. The discrete element rest angle was conducted with the best combination of parameters. The error of the test compared with the physical examination was 1%. The particles calibrated by simulation were subjected to the pneumatic suspension velocity test and particle mixing test. The test results matched the physical test results, which further verified the accuracy and applicability of the established discrete element model and parameters for coated powders.

Keywords: CFD; EDEM; discrete element method; parameter calibration

Citation: Ma, X.; Liu, M.; Hou, Z.; Li, J.; Gao, X.; Bai, Y.; Guo, M. Calibration and Experimental Studies on the Mixing Parameters of Red Clover Seeds and Coated Powders. *Processes* **2022**, *10*, 2280. https://doi.org/10.3390/pr10112280

Academic Editor: Ireneusz Zbicinski

Received: 29 September 2022
Accepted: 31 October 2022
Published: 3 November 2022

1. Introduction

Pelletizing coating technology makes it possible to mechanize the sowing of small grains of forage seeds and improves the seed germination survival rate [1]. At present, grassland restoration at home and abroad mainly adopts the method of scattering by drones and spraying by spraying machines [2]; some forage seeds are subject to size factors leading to low spraying efficiency and poor quality, and the use of seeds coated with pellets will improve the survival rate and germination rate after seed spraying. Red clover is often used as a green fertilizer plant and soil conservation plant, and is a high-quality forage grass, so the study of the red clover seed pelletizing coating process and technology for the restoration and replanting of degraded grassland to improve the construction of ecological civilization is of great importance.

In the coating process, the mixing motion between seed and seed, seed and powder, and the contact and collision relationship between them are complex [3]. Based on the theory of discrete element analysis, EDEM and Fluent software were used to numerically simulate the coating process of small grains of forage seeds, which is beneficial to reveal the kinematic and kinetic characteristics of germs, as well as the interaction between seeds and powders and the mixing mechanism, to improve and optimize the coating equipment and coating process parameters. Alizadeh [4] proposed the concept of JKR. (Johnson–Kendall–Roberts) surface energy to characterize the contact properties between wet particles in

computer simulations. Luo Shuai [5] carried out an experiment to calibrate the parameters of flour small particle matter using the stacking angle as the response value. Grim et al. [6] carried out a parametric calibration of the rolling friction coefficients of the dry and wet particles using the stacking angle as the response value. Li [7] determined the particle friction coefficient using the sliding plate sliding test method and verified it by discrete element simulation. Mohsin [8] calibrated the cohesion value between wet sand using the JKR model in EDEM to reproduce the actual behavior of damp sand. Li [9] calibrated the numerical simulation parameters for sandy soil particles with different water content by EDEM discrete element simulation combined with physical tests, and conducted the direct shear test for bonding parameters. Satoru [10] elaborated the kinematic collision velocity and collision number of charged particles of pneumatic conveying powders by the three-dimensional discrete element method. Yang [11] used a coupled CFD-DEM approach to study the coupling simulation model between large (5–30 mm) non-spherical particles. Xu [12] studied the effect of coalescence characteristics on powder suspension velocity in pneumatic conveying systems. Hao [13] used the discrete element method to calibrate the soil for Fluent and EDEM software in order to conduct a comparative study of wind–sand gas–solid two-phase flow tests and wind tunnel physical tests. Calibrating the forage seed and powder simulation parameters is beneficial to improve the accuracy of discrete element analysis theory in the process of forage seed pelletizing and coating research. There are few studies on the calibration of powder material parameters, and no studies on the calibration of discrete element simulation parameters for powders applicable to fluid–solid coupling simulation.

In order to study the physical properties applicable to seeds and powder particles in the fluid–solid coupling, this paper calibrates the contact parameters between powder and sources using the JKR parameter model in the discrete element method based on the particle scaling theory. The calibration results were used to conduct particle pneumatic suspension velocity tests and particle-mixing tests to verify the accuracy of the discrete element model parameters.

2. Materials and Methods

The group designed a cyclonic fluidized-bed small-grain forage seed pellet device, using the cyclonic fluidized bed to suspend the red clover seeds in the mixing chamber, and spray the atomized pellet agent onto the red clover seeds, so that the seed powder can be quickly contacted and evenly fused under the action of the air force to achieve the ideal pellet effect. The structure of the device is shown in Figure 1. The test was conducted with powder and red clover seeds prepared with soybean flour and diatomaceous earth at 1:1 ratio. One thousand red clover seeds were randomly selected to obtain the weight of single seeds by taking the average value of multiple measurements; vernier calipers were used to measure the external dimensions (length × width × height) of red clover seeds, and the density of seeds was measured by the immersion method; the moisture content of red clover seeds and powder were measured by the oven-drying method; the sieving method was used to determine the particle size of coated powder particles. The test was repeated several times. Dome basic physical parameters of red clover seeds and powder were measured, as shown in Table 1.

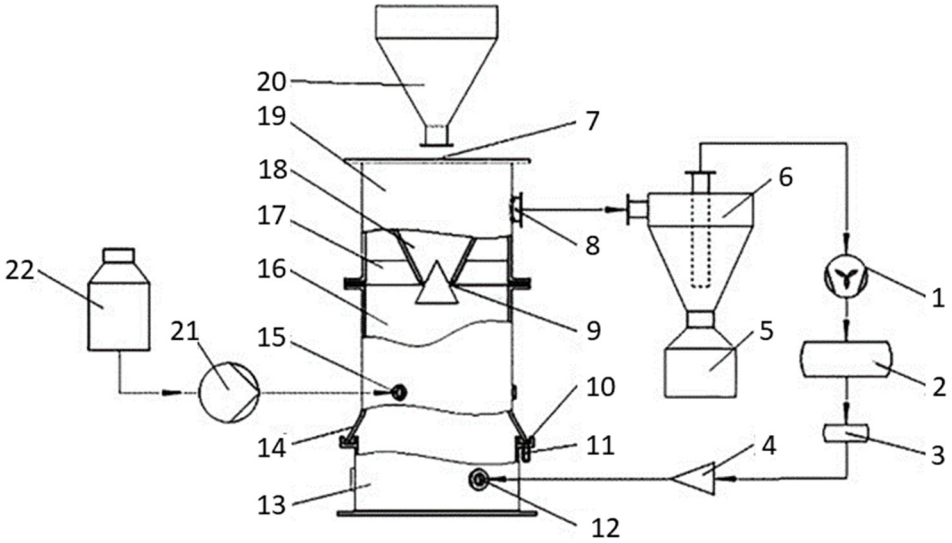

Figure 1. Structure diagram of a premixing machine for pelleted coated seed powder for small seeds. 1. Air compressors; 2. air pumps; 3. gas drainage device; 4. pressure valves; 5. waste collection device; 6. material recovery; 7. coating pan cover; 8. gas exports; 9. feeding devices; 10. sealing tape; 11. liquid medicine control valve; 12. air inlets; 13. intake pipe; 14. liquid medicine pipelines; 15. fluid medicine inlet; 16. coating material mixing zone; 17. sedimentation plates; 18. guide plate; 19. coating pot inside; 20. powder hopper; 21. peristaltic pump; 22. medicine tank.

Table 1. Basic physical properties of coated powder.

Physical Properties Parameters	Red Clover Seeds	Powder
Density/kg·m^{-3}	1279 ± 0.035	1833 ± 0.1
Water content/%	15 ± 0.352	1.54 ± 0.014
Particle size/mm	L: 2.0 ± 0.125 H: 1.5 ± 0.054 W: 1.1 ± 0.062	0.212

In general, in physical systems, physical quantities are often not all independent of each other. Most physical quantities can be derived from identified independent or fundamental quantities, with only a few independent or total material amounts. In conventional S.I. systems, the three commonly used fundamental physical quantities are length (L), mass (M), and time (T), and the other physical quantities are derived according to the units of the model [14]. In this study, density is the basic material parameter that can be directly obtained, and the commonly used basic physical quantities of density (ρ), length (L), and time (T) are selected as the basic scaling quantities. The other physical quantities are derived by scaling relations based on the three basic quantities. The scaling factors of the fundamental quantities—density factor (ρ), length factor (L), and time factor (T)—are:

$$\lambda_\rho = 1, \lambda_L = h, \lambda_T = h \quad (1)$$

The other physical quantities in the physical model derived from Equation (1) are shown in Table 2.

Table 2. Basic physical properties of coated powder.

Variables	Symbol	Scale	Scaling Ratio (λ)	Category
Length	L	(L)	h	Basic
Time	T	(T)	h	Basic
Density	ρ	(ρ)	1	Basic
Area	A	$(L)^2$	h^2	Geometry
Volume	V	$(L)^2$	h^3	Geometry
Displacement (amount of overlap)	u	(L)	h	Motion
Velocity	v	$(L)\ (T)^{-1}$	1	Motion
Force	F	$(\rho)\ (L)^4(T)^{-2}$	h^2	Forces
Stiffness	k	$(\rho)\ (L)^3(T)^{-2}$	h	Force
Mass	M	$(\rho)\ (L)^2(T)^{-2}$	h^3	Material
Young's modulus	E	$(\rho)\ (L)^3(T)^{-2}$	1	Material

The scaling factors of Young's modulus E and velocity v can be found to be 1. For the JKR contact model in this study, which is non-scale invariant, the k in the linear model $F = ku$ is scaled to hk to produce a scale-invariant scaled linear contact model by considering it in conjunction with Equation (1). The stiffness $\overline{k}$ of the scaled model is:

$$\overline{k} = hk \tag{2}$$

This leads to the derivation of the scaled model stiffness $\overline{k}$ and the scaling factor of the scaled model's Young's modulus $\overline{E}$ as:

$$\begin{array}{c} k = [\rho][\mathrm{L}]^3[\mathrm{T}]^{-2} \Rightarrow \lambda_k = h \Rightarrow \lambda_{\overline{k}} = h^2 \\ \overline{E} = \mathrm{L}\overline{k}u/A \Rightarrow [E] = [\mathrm{L}]\overline{k}[T]^{-2} \Rightarrow \lambda_{\overline{E}} = h \end{array} \tag{3}$$

From the dimensional analysis results, it can be seen that when density, length, and time are the fundamental quantities, the parameters such as contact stiffness, elastic modulus, and recovery coefficient are varied with the variable diameter scaling and need to be determined by calibration. The density is kept constant to decide the linear relationship between contact stiffness and particle size, and the velocity is kept constant for the accuracy of the subsequent simulation tests. The JKR normal elastic force F_{JKR} is calculated as:

$$F_{JKR} = \frac{4E^*R^3}{3R^*} - 4\sqrt{\pi\Delta\gamma E^*R^3} \tag{4}$$

$$\delta = \frac{R^2}{R^*} - \sqrt{\frac{4\pi\gamma R}{E^*}} \tag{5}$$

where F_{JKR} is the average modulus of elasticity in N; R is the radius of the contact circle between two particles in meters; E^* is the equivalent modulus of elasticity in Pa; R^* is the equal radius in meters. $\Delta\gamma$ is the particle surface energy in J/m^2 and δ is the amount of overlap in meters. Whether the particles are in direct contact, this model provides cohesion between the particles, and the two particles have non-zero cohesion between the maximum [15]. The gap δ_c is:

$$\delta_c = \frac{R^2}{R^*} - \sqrt{\frac{4\pi\gamma R}{E^*}} \tag{6}$$

$$R_c = \left[\frac{9\pi\gamma R^2}{2E^*} - \frac{3-2\sqrt{2}}{4}\right]^{\frac{1}{3}} \tag{7}$$

where R_c is the radius of the contact circle at the maximum gap normal to the two particles in meters. Cohesion reaches a maximum when the particle gap is less than δ_c:

$$F_p = -\frac{3}{2}\pi\gamma R^* \tag{8}$$

It is shown that the interparticle cohesion is proportional to the scaled particle radius and that the interparticle contact surface area increases as the particle radius increases. In the parameter JKR setting, JKR varies with scaling and is determined by calibration according to its range.

Poisson's ratio is one of the essential parameters of the simulation test. Because the shape of red clover seeds is different and their size is minimal, it is difficult to obtain their Poisson's ratio and shear modulus by conventional experimental methods; therefore, their Poisson's ratio and shear modulus range are obtained from literature [16]. Poisson's ratio of red clover seeds ranges from 0.2 to 0.4, and the shear modulus ranges from 5 to 20 Mpa. Poisson's ratio and the shear modulus were calibrated at a later stage. The Poisson's ratio of powder was obtained by the fast shear test with a Nanjing Z.J.-type straight shear instrument, and Poisson's ratio of powder was 0.296. The shear modulus of the powder was obtained from Equation (9), and the elastic modulus of the powder was 7.78×10^7.

$$G = -\frac{E}{2(1+\mu)} \tag{9}$$

where G is the powder shear modulus in Pa, E is the powder elastic modulus in Pa, and μ is the powder Poisson's ratio.

Combined with domestic and international literature and referring to the built-in database of EDEM software [17,18], the powder simulation parameters were obtained, as shown in Table 3.

Table 3. Discrete element simulation test parameters.

Simulation Parameters	Values	Simulation Parameters	Values
Poisson's ratio of red clover seeds	0.3	Poisson's ratio of powder	0.296
Shear modulus of red clover seeds / Pa	1.25×10^7	Powder shear modulus/Pa	3×10^7
Red clover seed–seed collision recovery coefficient	0.50	Red clover seeds–steel plate collision recovery coefficient	0.57
Red clover seed–seed static friction coefficient	0.605	Red clover seeds-static friction coefficient of steel plate	0.388
Red clover seed–seed rolling friction coefficient	0.637	Red clover seeds-rolling friction coefficient of steel plate	0.37

The powder particle and red clover seed particle simulation models were established in discrete element simulation software. The powder particle adopts a single-ball model, as shown in Figure 2a. In order to minimize the simulation error and obtain a reasonable and practical simulation time, the coated powder particles were scaled six times from the physical test values for simulation based on the particle scaling theory [19,20]. The discrete element simulation model of red clover seed particles was established by multi-sphere aggregation, and the model dimensions were adopted from physical test values. The seed edges were rounded, as shown in Figure 2b. The Hertz–Mindlin with JKR contact model was selected for the powder simulation test. The calibration test uses an FT-104B rest angle meter, the particle generation method is set to dynamic, 5 g of powder particles are generated, the grid size is $3R_{min}$, and the total simulation time is set to 5 s.

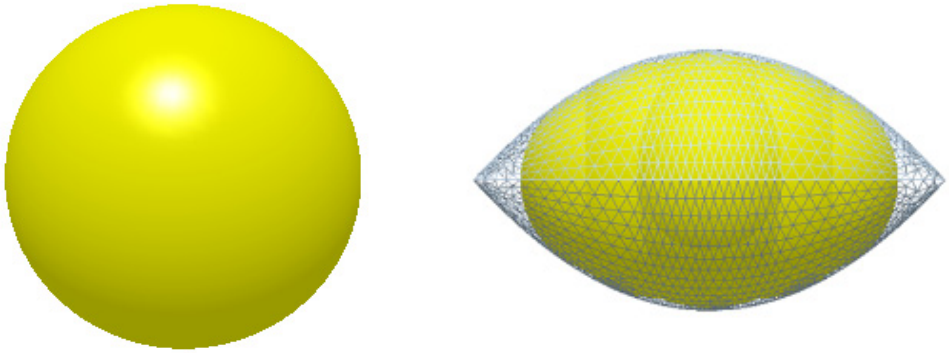

(**a**) (**b**)

Figure 2. Powder and red clover seed simulation models. (**a**) Powder particles; (**b**) red clover seed pellets.

The CFD-DEM fluid–solid coupling method simulates and investigates the motion state of red clover seeds and powder. In the numerical simulation process, the standard k-ε model is chosen as the turbulence model. In the solution scheme, the SIMPLE algorithm is determined to solve the momentum equation to obtain the most accurate convergence results, and the residual convergence criterion is 10^{-5}.The fluid–solid coupling algorithm requires that the volume of particles in the flow field be smaller than the delineated grid volume, so the minimum grid cell size is set to 1.5 mm. At this time, the total number of grids in the fluid calculation domain is 2,923,000; the average mass of the grids is greater than 0.89 [21,22].

The Eulerian describes the coupling between the material and the airflow. The forces on the particles relative to the fluid phase are considered, including the exchange of mass, momentum, and energy [23]. The gas flow process in the coating process satisfies the mass conservation law and momentum conservation law, where the gas phase continuity equation and momentum equation are:

$$\frac{\partial(\varphi\rho)}{\partial t} + \nabla(\varphi\rho u) = 0 \tag{10}$$

$$\frac{\partial(\varphi\rho)}{\partial t} + \nabla(\varphi\rho u) = -\nabla \mathrm{p} + \nabla(\eta\varphi\nabla u) - \varphi\rho g - S \tag{11}$$

where φ is the volume fraction occupied by the gas, t is time in seconds; ρ is the gas density in kg/m^3; u is the gas velocity in m/s; p is the gas pressure in Pa; g is the acceleration of gravity in m/s^2; η is the gas viscosity in Pa·s; S is the drag momentum sink.

The coupling between two phases—the gas phase, and particle phase—is achieved by calculating the drag momentum sink. The expression of the drag momentum sink S is:

$$S = \frac{\sum_i^n F_D}{V} \tag{12}$$

Among them:

$$F_D = 0.5 C_D \rho A \left|u - u_p\right| (u - u_p) \tag{13}$$

$$Re = \frac{v_0 \rho d_s}{\mu} \tag{14}$$

$$C_D = \begin{cases} \frac{24}{Re}, & \left(d_s \le 2.2\left[\frac{\mu^2}{\rho(\rho_s-\rho)}\right]^{\frac{1}{3}}\right) \\ \frac{10}{\sqrt{Re}}, & \left(2.2\left[\frac{\mu^2}{\rho(\rho_s-\rho)}\right]^{\frac{1}{3}} \le d_s \le 20.4\left[\frac{\mu^2}{\rho(\rho_s-\rho)}\right]^{\frac{1}{3}}\right) \\ 0.44, & \left(20.4\left[\frac{\mu^2}{\rho(\rho_s-\rho)}\right]^{\frac{1}{3}} \le d_s \le 1100\left[\frac{\mu^2}{\rho(\rho_s-\rho)}\right]^{\frac{1}{3}}\right) \end{cases} \quad (15)$$

where F_D is the fluid resistance of the particle in N; V is the volume of the grid cell in m^3; C_D is the traction coefficient; A is the projected area of the particle in m^2; u_p is the particle velocity in m/s; ρ_s is the particle density in kg/m^3; Re is the Reynolds number; d_s is the equivalent diameter of the particle in meters; μ is the aerodynamic viscosity coefficient in Pa·s.

In the EDEM-FLUENT coupling module, the Ergun, Wen, and Yu (Gidaspow) model is selected for the interaction force between two phases to more accurately reflect the interaction between particles and fluid in this test; this model is used in this paper to simulate the experimental study. The calculation method of this model is as follows.

$$F_{Gidaspow} = \begin{cases} 150\frac{{\varepsilon_s}^2\mu_g}{\varepsilon_g {d_p}^2} + 1.75\frac{\varepsilon_s\rho_g\left|\vec{v_s}-\vec{v_g}\right|}{d_p}, \varepsilon_g \le 0.8 \\ \frac{3}{4}C_D\frac{\varepsilon_s\varepsilon_g\rho_g\left|\vec{v_s}-\vec{v_g}\right|}{d_p}\varepsilon_s^{-2.65}, 0.8 \le \varepsilon_g \le 1 \end{cases} \quad (16)$$

where ϵ_g is the volume fraction of the gas; ϵ_s is the volume fraction of the particles; μ_g is the viscosity coefficient of the gas; ρ_g is the density of the gas in kg/m^3; v_g is the velocity of motion of the gas in m/s; v_s is the velocity of motion of the particles in m/s; and d_p is the diameter of the particles in meters.

3. Results

In the process of the seed pellet coating test, there are a large number of mutual contacts between seed and powder, and these contact parameters affect the accuracy of the test in the simulation, so the collision recovery coefficient, static friction coefficient, and rolling friction coefficient of seed–powder used in the trial were calibrated. A control test was used to determine the seed–powder collision recovery coefficient, static friction coefficient, and rolling friction coefficient, in turn, and the rebound height of seeds falling freely on the powder plate was recorded with a high-speed camera. The average seed rebound height obtained was 8.01mm. Only the seed–powder collision recovery coefficient x_1 would affect the seed rebound height y_1 in the test, and different values of x_1 were set in the EDEM software to obtain the corresponding of y_1, where the error between y_1 and 8.01 mm is e_1; the angle at which the seeds appear to slide on the powder plate was measured with the inclinometer and the angle of rotation of the inclinometer was obtained as 36°. The corresponding rise of the inclinometer, y_2, was obtained by setting different values of the static friction coefficient x_2 of the seed–powder in the EDEM software, where the error between y_2 and 36° is e_2. The horizontal rolling distance of the sources was 69.2 mm after sliding down the powder plate at a greater angle, and the corresponding horizontal rolling distance y_3 was obtained by setting different values of the rolling friction coefficient x_3 of the seed–powder in the EDEM software, where the error between y_3 and 69.2 mm was e_3. The above simulation test scheme and results are shown in Table 4.

Table 4. Test design and results.

No.	x_1	y_1/mm	e_1/%	x_2	y_2/°	e_2/%	x_3	y_3/mm	e_3/%
1	0.1	2.499	220.528	0.7	20.4	56.13	0.2	114.6	39.62
2	0.15	4.615	73.564	0.72	22.86	39.33	0.22	93.12	25.69
3	0.2	6.09	31.527	0.74	24.12	32.05	0.24	81.51	15.10
4	0.25	8.502	5.787	0.76	29.04	9.68	0.26	63.08	9.70
5	0.3	9.809	18.340	0.78	32.76	2.78	0.28	56	23.57
6	0.35	13.39	40.179	0.8	37.8	15.74	0.3	39.88	73.52

The test factors and data in Table 4 were fitted to obtain the relationship between the contact parameters and physical test values between red clover seeds and powder. The fitted curves are shown in Figure 3.

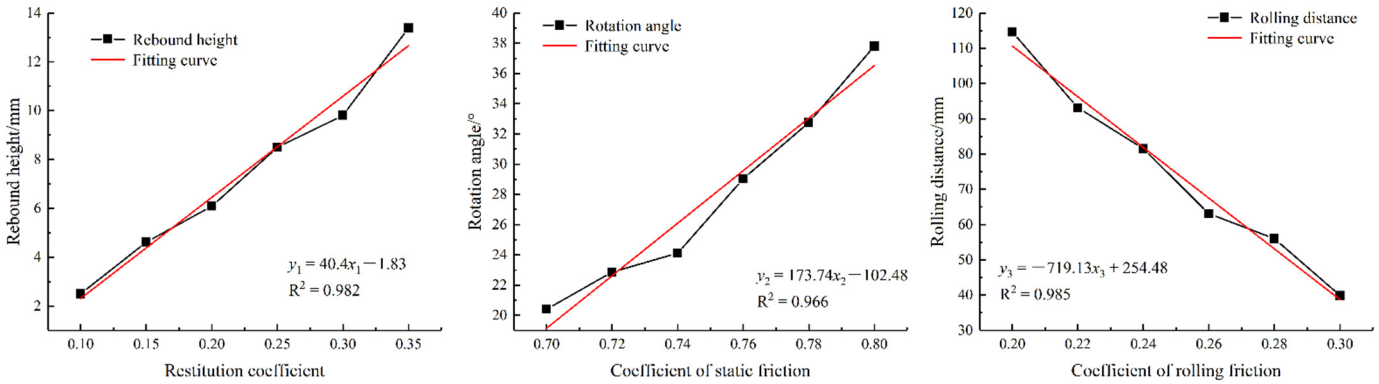

(**a**) (**b**) (**c**)

Figure 3. Fitting curves of each contact parameter to the corresponding physical test values. (**a**) The fitting curves of seed–powder collision recovery coefficient x_1 and seed rebound height y_1; (**b**) fitting curve of static friction coefficient x_2 of seed–powder and rotation angle y_2 of seed inclinometer; (**c**) seed–powder rolling friction coefficient x_3 and seed horizontal rolling distance y_3 fitting curve.

The coefficients of determination R^2 of the curve-fitting equations in the figure are all close to 1, indicating the high reliability of the equation fitting. The seed–powder collision recovery coefficient of 0.246, static friction coefficient of 0.776, and rolling friction coefficient of 0.255 were obtained by substituting the physical test values into the fitted curves.

The powder rest angle test was carried out using an FT-104B rest angle tester, and the powder was poured from the top of the funnel and allowed to fall freely by the injection method. The powder's rest angle was measured using the digital display meter when the stacking angle remained unchanged, The test was repeated ten times, and the average value was obtained as 41.69° ± 0.79. The rest angle simulation model was established using 3D modeling software and imported into EDEM for the simulation test, and the profile curve was extracted and linearly fitted by means of image processing to obtain the rest angle. The results of the physical test compared with the simulation test are shown in Figure 4. The Plackett–Burman simulation test design was carried out according to the parameters shown in Table 5, and the results were obtained as shown in Table 6.

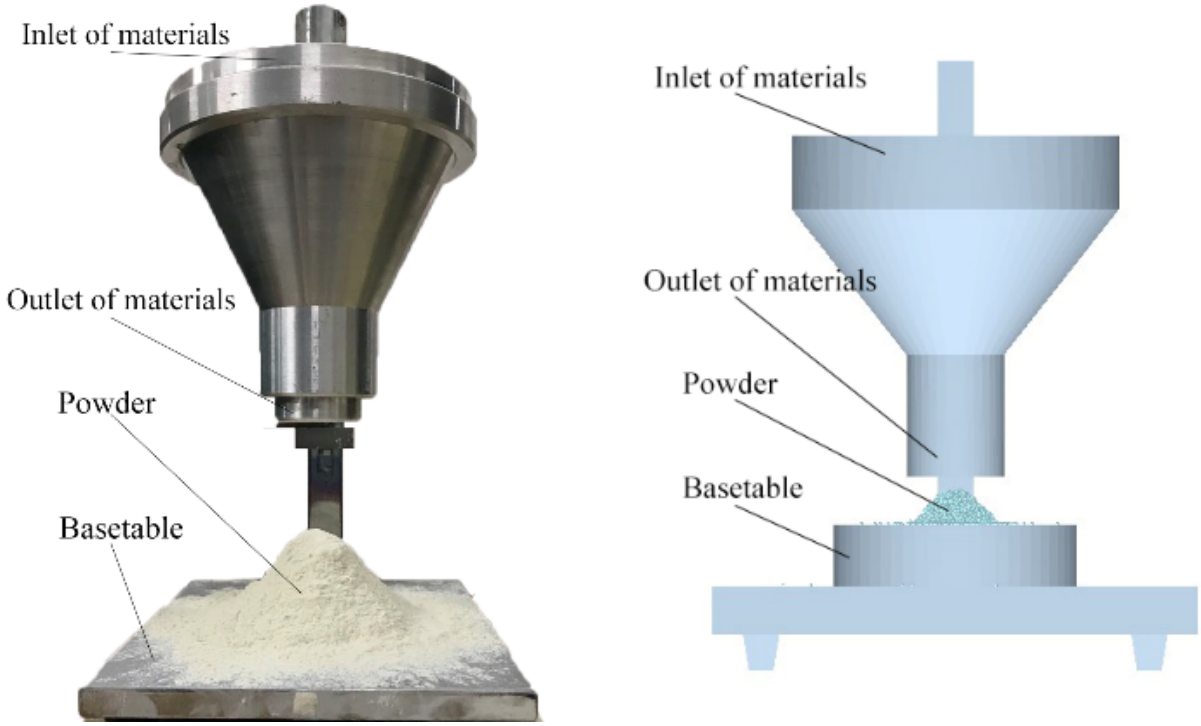

(**a**) (**b**)

Figure 4. The angle of repose test: (**a**) FT-104B resting angle tester; (**b**) resting angle simulation model.

Table 5. Range of simulation test parameters.

Physical Property Parameters	Low Level (−1)	High Level (+1)
Powder–powder restitution coefficient *A*	0.05	0.25
Powder–powder static friction coefficient *B*	0.7	0.9
Powder–powder rolling friction coefficient *C*	0.25	0.45
Powder–steel plate restitution coefficient *D*	0.05	0.25
Powder–steel plate static friction coefficient *E*	0.62	0.82
Powder–steel plate rolling friction coefficient *F*	0.19	0.39
JKR surface energy *G*	0.1	0.3

Table 6. Plackett–Burman trial design and results.

No.	*A*	*B*	*C*	*D*	*E*	*F*	*G*	Repose Angle θ/(°)
1	1	1	−1	1	1	1	−1	30.86
2	−1	1	1	−1	1	1	1	48.00
3	1	−1	1	1	−1	1	1	49.16
4	−1	1	−1	1	1	−1	1	39.11
5	−1	−1	1	−1	1	1	−1	42.73
6	−1	−1	−1	1	−1	1	1	41.45
7	1	−1	−1	−1	1	−1	1	44.82
8	1	1	−1	−1	−1	1	−1	33.91
9	1	1	1	−1	−1	−1	1	44.41
10	−1	1	1	1	−1	−1	−1	38.53
11	1	−1	1	1	1	−1	−1	43.24
12	−1	−1	−1	−1	−1	−1	−1	32.78
13	0	0	0	0	0	0	0	43.74

ANOVA was performed on the results of the Plackett–Burman test, and the significant simulation test parameters were obtained, as shown in Table 7. As can be seen from

Table 7, G (JKR surface energy) and C (powder–powder rolling friction coefficient) have $p < 0.01$, which has highly significant effects on the rest angle of the simulation test; B (powder–powder static friction coefficient) has $p < 0.05$, which has a substantial impact on the rest angle of the simulation test; other simulation tests have $p < 0.05$, which has significant effects on the rest angle of the simulation test. coefficient) with $p < 0.05$, which has a substantial impact on the rest angle of the simulation test; other simulation test parameters with $p > 0.05$, which has a minimal effect on the rest angle of the simulation test. The significant factors were ranked as G (JKR surface energy) > C (powder–powder rolling friction coefficient) > B (powder–powder static friction coefficient), according to the Plackett-Burman test results for the screened three significant parameters to design the steepest climb test, the powder rest angle test error as the response value, to find the optimal range of the three factors, the experimental design and results are shown in Table 8.

Table 7. Significance analysis of Plackett–Burman test parameters.

Parameters	DF	Sum of Squares	*F*-Value	*p*-Value
A	1	1.20	0.31	0.6084
B	1	31.23	8.00	0.0474 *
C	1	155.09	39.72	0.0032 **
D	1	1.54	0.39	0.5640
E	1	6.05	1.55	0.2812
F	1	0.86	0.22	0.6626
Ge	1	168.00	43.03	0.0028 **

Note: ** in Table 7 indicates that the impact is highly significant ($p < 0.01$), and * indicates that the effect is significant ($p < 0.05$).

Table 8. The design scheme and results of the steepest climbing test.

No.	Powder–Powder Static Friction Coefficient *B*	Powder–Powder Rolling Friction Coefficient *C*	JKR Surface Energy *G*	Relative Error %
1	0.9	0.25	0.1	22.91
2	0.86	0.29	0.14	0.50
3	0.82	0.33	0.18	2.64
4	0.78	0.37	0.22	4.41
5	0.74	0.41	0.26	6.86
6	0.7	0.45	0.30	31.66

Table 8 shows that the relative error of the rest angle decreases and then increases, and the relative error of the rest angle is the smallest at test level 2. Then, the test design is carried out in the subsequent test with test level 2 as the center point and test levels 1 and 3 as low and high levels, respectively. Based on the steepest climb test results, the screened significance parameters were subjected to the Box–Behnken test. The experimental design scheme and results are shown in Table 9. The response surface Box–Behnken test results are shown in Figure 5.

Table 9. Box–Behnken test protocol and results.

No.	*B*	*C*	*G*	Repose Angle θ/(°)
1	−1	−1	0	36.41
2	1	−1	0	36.96
3	−1	1	0	42.25
4	1	1	0	42.33
5	−1	0	−1	32.76
6	1	0	−1	37.86
7	−1	0	1	38.91
8	1	0	1	38.43
9	0	−1	−1	30.62
10	0	1	−1	38.69
11	0	−1	1	37.21
12	0	1	1	39.96
13	0	0	0	40.55
14	0	0	0	41.17
15	0	0	0	41.53
16	0	0	0	41.31
17	0	0	0	41.7

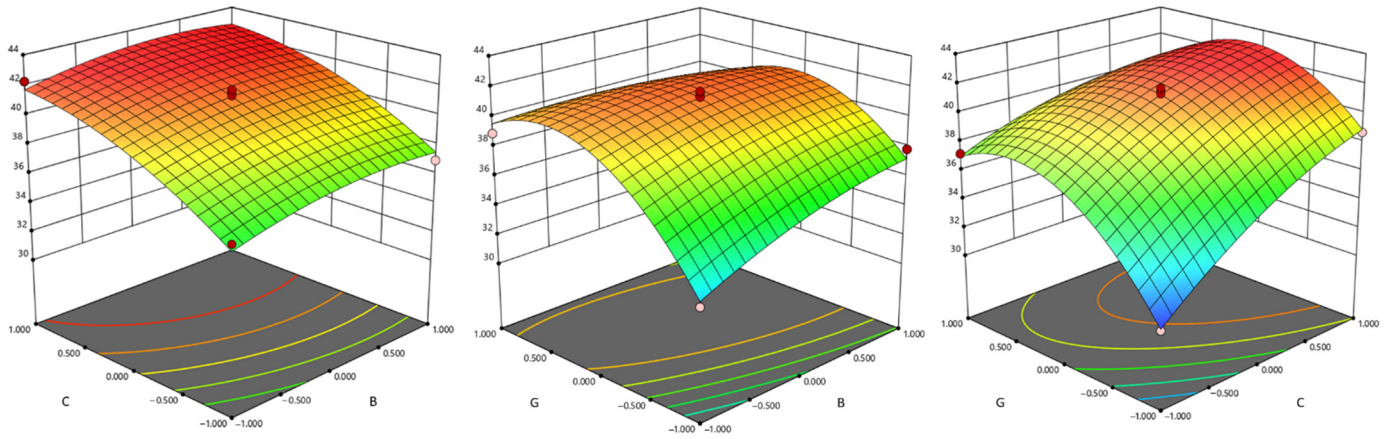

(**a**) (**b**) (**c**)

Figure 5. Box–Behnken test results response surface. (**a**) Effect of powder–powder static friction coefficient and rolling friction coefficient on resting angle of powder; (**b**) effect of powder–powder static friction coefficient and JKR surface energy on powder resting angle; (**c**) effect of powder–powder static friction coefficient and JKR surface energy on powder resting angle.

The results of the Box–Behnken test ANOVA are shown in Table 10, where *C* (powder–powder rolling friction coefficient), *G* (JKR surface energy), *BG* (powder–powder static friction coefficient, and JKR surface energy interaction term), *CG* (powder–powder rolling friction coefficient and JKR surface energy interaction term), and G^2 (JKR surface energy quadratic term) have highly significant effects on the powder rest angle. *B* (powder–powder static friction coefficient) and C^2 (powder–powder rolling friction quadratic term) have substantial effects on the powder rest angle, and the rest of the parameters have insignificant effects on the powder rest angle. According to the response surface analysis, it can be seen that the powder–powder rolling friction coefficient and JKR surface energy interaction term, and the powder–powder static friction coefficient and JKR surface energy interaction term have an extremely significant effect on the powder rest angle, and the powder–powder static friction coefficient and powder–powder static friction coefficient interaction term have a negligible effect on the powder rest angle. In order to find the optimal combination of parameters for the powder rest angle simulation, a second-order regression equation for the relative error of factors and rest angle was fitted as follows:

$$\theta = 41.25 + 0.66B + 2.75C + 1.82G - 0.11BC - 1.4BG - 1.33CG - 0.7B^2 - 1.07C^2 - 3.56G^2 \quad (17)$$

Table 10. Box–Behnken test regression model analysis of variance.

Source	Mean Square	Degree of Freedom	Sum of Square	*p*-Value
Model	18.85	9	169.61	<0.0001 **
B	3.45	1	3.45	0.0244 *
C	60.67	1	60.67	<0.0001 **
G	26.57	1	26.57	<0.0001 **
BC	0.0552	1	0.0552	0.7281
BG	7.78	1	7.78	0.0036 **
CG	7.08	1	7.08	0.0046 **
B^2	2.05	1	2.05	0.0634
C^2	4.80	1	4.80	0.0119 *
G^2	53.51	1	53.51	<0.0001 **
Residual	0.4218	7	2.95	
Lack of fit	0.7238	3	2.17	0.1190
Pure error	0.1952	4	0.7809	
Sum		16	172.56	

Note: ** in Table 10 indicates that the impact is highly significant ($p < 0.01$), and * indicates that the effect is significant ($p < 0.05$).

The second-order regression equation was optimized by using the rest angle of the physical test as the target value to obtain a set of parameters similar to the mean value of the physical examination; the powder–powder static friction coefficient was 0.887, the powder–powder rolling friction coefficient was 0.319, and the JKR surface energy was 0.162 J/m^2. The EDEM powder rest angle simulation test was conducted using the solved parameter combinations. The average value of 41.27° was obtained from five tests, which is only a 1% relative error to the physical test. The experimental comparison is shown in Figure 6.

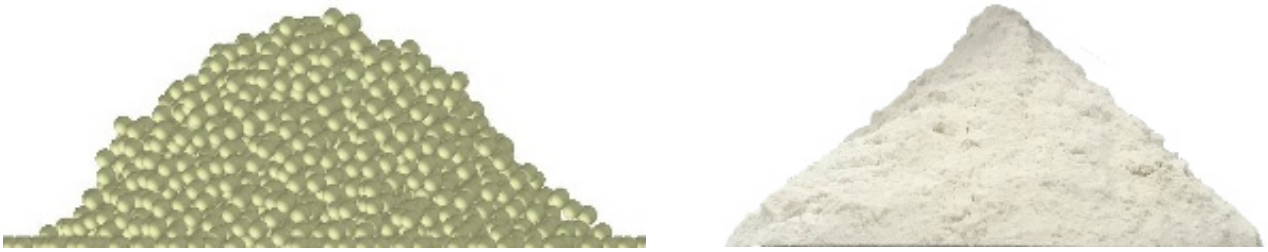

(**a**) (**b**)

Figure 6. Test comparison of the angle of repose of powder. (**a**) Simulation test results; (**b**) physical test results.

4. Discussion

To further verify the accuracy and applicability of the numerical simulation parameters taken, a seed–powder mixing test under the action of the air force was carried out. The particle plant was set up in the coating pot using EDEM software, and two kinds of particles—seeds and powder—were generated from the particle plant and fell freely. Since the two types of particles had different suspension velocities, the material particles showed different motion trajectories under the action of airflow. In Fluent software, the airflow velocity at the airflow inlet was set to 2 m/s and 8 m/s, respectively. Short diagrams of the two airflow velocities at 2 s are shown in Figure 7, where gray is the seed particles, and magenta is the powder particles. From Figure 7, it can be seen that when the airflow speed is 2 m/s, the powder particles appear to be suspended, but the seed particles have a larger mass and do not reach the suspension condition; when the airflow speed is 8 m/s, both seed and powder particles are blown to the top of the coating pot; the value of the

subsequent airflow speed should be selected in the range of 2–8 m/s. The results of this simulation were compared with the results within the literature [24,25]. Zhao found seed suspension speed physical test results of 3.06–5.77 m/s for alfalfa, and simulation results match. Li tested of alfalfa seeds with suspension speed of 5.06 m/s, and the suspension speed value was within the range of simulation results.

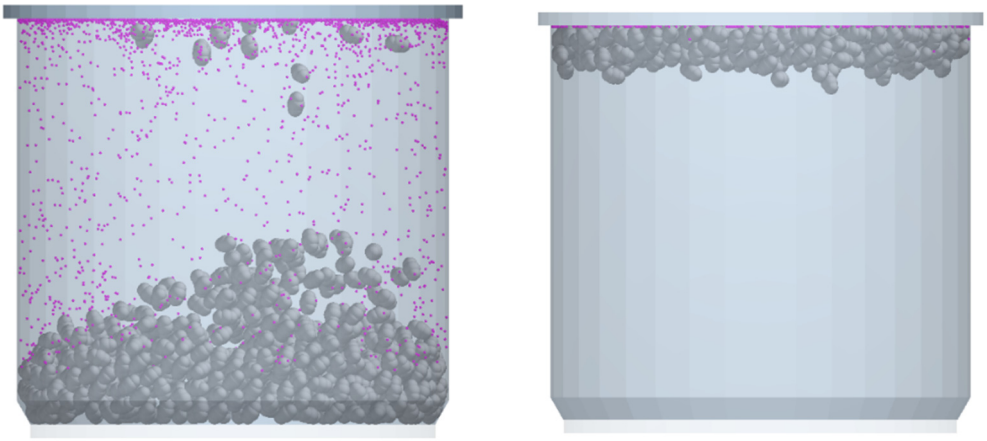

(**a**) (**b**)

Figure 7. Material particle position transient map. (**a**) When the air velocity is 2 m/s, two material particles are suspended; (**b**) when the air velocity is 8 m/s, two types of material particles are suspended.

In the current situation where the pelletized coating cannot be fully simulated, the subsequent seed pelletizing effect is judged by observing the mixing between the particles. In order to quantitatively describe the particle-mixing effect, most scholars use the coefficient of variation of powder particles as an evaluation index, and the coefficient of variation, which takes into account the average value of the data, is more suitable for application to axial mixing. Due to the existence of the pneumatic force, seeds, powder, and other materials in the coating pot are not only limited to axial mixing, but also take into account radial mixing by the grid division sampling method on radial images. This paper used the coefficient of variation of powder particles and the Lacey index algorithm to evaluate the mixing of red clover seeds and powder. The relationship between the number of particle positions during mixing was counted by the EDEM software post-processing Grid Bin Group module, and the grid cell size for counting the number of particles was five times the average diameter of the particles [26]. The smaller the powder coefficient of variation value, the better the mixing effect of the two materials; the closer the value of the Lacey index to 1, the better the mixing development. The figure shows the powder coefficient of variation and Lacey index for five different airflow velocity conditions. The coefficient of variation CV of the powder is calculated by Equation (18), and the Lacey index algorithm M is calculated by Equation (19).

$$C_v = \frac{S_x}{\overline{x}} \tag{18}$$

$$\mathrm{M} = \frac{S_0^2 - S^2}{S_0^2 - S_r^2} \tag{19}$$

where S_x is the standard deviation of all powder particles; $\overline{x}$ is the mean of the particles; S^2 is the actual mixing variance of the two particles; ${S_0}^2$ is the mixing variance at complete separation; ${S_r}^2$ is the utterly random mixing variance of the two particles.

From Figure 8a, it can be seen that the overall trends of the coefficient of variation in the mixing process at different airflow velocities all decrease with the increase of time, indicating that the mixing between seed and powder gradually stabilizes with time. When the particles were mixed from the start to 0.25 s, the variation of the coefficient of variation

was not regular. When the time was 0.2–0.5 s, the powder coefficient of variation began to stabilize. Different approximations of the coefficient of variation at different airflow speeds began to appear, indicating that the mixing effect of seed–powder at different airflow speeds was different, which further suggested that the mixing between seeds and powder tended to stabilize with the increase of time. In general, an airflow speed of 3.5 m/s required a shorter time and a smaller coefficient of variation to achieve the same mixing uniformity. The degree of mixing was better than other airflow speeds. As shown in Figure 8b, the Lacey index shows an overall trend for different airflow velocities with increasing time. From the beginning of particle mixing to the time of 0.25 s, the Lacey index and the coefficient of variation are not regular, which indicates that the material at this stage is not stable by the pneumatic action state, and the mixing effect is not ideal. When the time is 0.2–0.5 s, the Lacey index is the largest when the airflow speed is 3.5 m/s, indicating that when the airflow speed is 3.5 m/s, the material mixing effect is the best. The Lacey index is close to the air velocity of 2 m/s and 5 m/s, which means that the air velocity that is too large or too small will change the material mixing effect. When the airflow speed is 8 m/s, the lift force inside the coating pot is larger than the gravity of the seeds and powder due to the considerable inlet wind speed, so the seeds and powder are all concentrated in the narrow space at the top of the coating pot and cannot fill the inside of the bank, resulting in insufficient material mixing. The coefficient of powder variation and the Lacey index showed that the best mixing effect of seeds and powder was achieved when the airflow speed was 3.5 m/s. A physical test of pelletizing coating with changing airflow was carried out, and the test results showed that the highest passing rate of pelletizing was at 3.5 m/s. This indicates that the model parameters are accurate, the simulation test can guide the pelletizing coating test, and the parameters calibrated in this paper can be used in the subsequent simulation test.

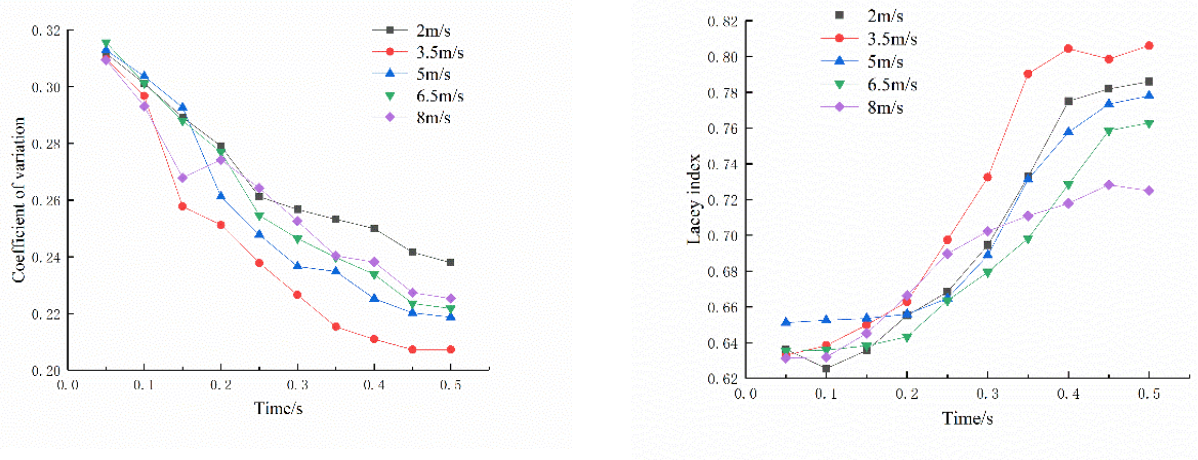

(**a**) (**b**)

Figure 8. Effect of air velocity on particle-mixing uniformity. (**a**) Coefficient of variation of particles at different airflow velocities; (**b**) Lacey index of particles at different airflow velocities.

5. Conclusions

A DEM powder particle model for CFD-DEM fluid–solid coupled simulation was established based on particle scaling theory. The calibrated results can improve the accuracy of the pill granulation coating simulation test and promote the optimization of parameters in the pill granulation coating test. Calibrating the discrete element model applicable to the fluid–solid coupling simulation provides an essential reference for other practical CFD-DEM coupling simulation studies.

1. A powder model in the EDEM simulation process was constructed based on particle scaling, and the collision recovery coefficient of seed–powder, static friction coefficient of seed–powder, and rolling friction coefficient of seed–powder were obtained by comparing the simulation test with the physical examination.

2. The Plackett–Burman test in EDEM software was used to screen the parameters, with a significant effect on powder rest angle, and the optimal combination of powder simulation parameters was found by the Box–Behnken test. The error of the powder simulation rest angle test using this combination of parameters was 1% compared to the physical examination.
3. The pneumatic suspension velocity test using the calibrated particles verified that the simulation test results were accurate for subsequent tests; in the particle mixing test, under the action of pneumatic force, the coefficient of variation and Lacey index were used to measure the effect of seed–powder mixing. The results corresponded to the physical test, indicating that the parameter calibration results were accurate for subsequent simulation tests.

Author Contributions: Conceptualization, Z.H.; methodology, X.M. and M.L.; software, M.L. and X.G.; validation, Y.B.; investigation, M.G.; writing—original draft preparation, X.M. and M.L.; writing—review and editing, X.M. and J.L. All authors have read and agreed to the published version of the manuscript.

Funding: This research was funded by the National Natural Science Foundation of China grant number 41661058. This research was funded by the Natural Science Foundation of Inner Mongolia Autonomous Region grant number 2018MS05023. This research was funded by the Program for improving the Scientific Research Ability of Youth Teachers of Inner Mongolia Agricultural University.

Institutional Review Board Statement: Not applicable.

Informed Consent Statement: Not applicable.

Data Availability Statement: Data are contained within the article. All the code generated or used during the study are available from the corresponding author.

Conflicts of Interest: The authors declare no conflict of interest.

References

1. Yi, Q.; Zhi, C.; Zhanfeng, H.; Tao, S.; Longkai, M.; Zhiwei, S. Numerical simulation and experiment on improving pelleted coating of forage grass seeds by vibration force field. *Trans. Chin. Soc. Agric. Eng.* **2017**, *33*, 86–93.
2. Zhanfeng, H.; Nianzu, D.; Zhi, C.; Yi, Q.; Xiwen, Z. Measurement and calibration of physical property parameters for Agropyron seeds in a discrete element simulation. *Trans. Chin. Soc. Agric. Eng.* **2020**, *36*, 46–54.
3. Liu, M.; Hou, Z.; Ma, X.; Zhang, X.; Dai, N. Determination and Testing of Pelletized Coated Particles. *INMATEH Agric. Eng.* **2022**, *66*, 247–256. [CrossRef]
4. Alizadeh, M.; Asachi, M.; Ghadiri, M.; Bayly, A.; Hassanpour, A. A methodology for calibration of DEM input parameters in simulation of segregation of powder mixtures, a special focus on adhesion. *Powder Technol.* **2018**, *339*, 789–800. [CrossRef]
5. Luo, S.; Yuan, Q.; Gouda, S. Parameters Calibration of Vermicomposting Nursery Substrate with Discrete Element Method Based on JKR Contact Model. *Trans. Chin. Soc. Agric. Eng.* **2018**, *49*, 343–350.
6. Grima, A.P.; Wypych, P.W. Development and validation of calibration methods for discrete element modelling. *Granul. Matter* **2010**, *13*, 127–132. [CrossRef]
7. Li, Y.; Xu, Y.; Thornton, C. A comparison of discrete element simulations and experiments for 'sandpiles' composed of spherical particles. *Powder Technol.* **2005**, *160*, 219–228. [CrossRef]
8. Ajmal, M.; Roessler, T.; Richter, C.; Katterfeld, A. Calibration of cohesive DEM parameters under rapid flow conditions and low consolidation stresses. *Powder Technol.* **2020**, *374*, 22–32. [CrossRef]
9. Li, J.; Xie, S.; Liu, F.; Guo, Y.; Liu, C.; Shang, Z.; Zhao, X. Calibration and Testing of Discrete Element Simulation Parameters for Sandy Soils in Potato Growing Areas. *Appl. Sci.* **2022**, *12*, 125. [CrossRef]
10. Watano, S. Mechanism and control of electrification in pneumatic conveying of powders. *Chem. Eng. Sci.* **2006**, *61*, 2271–2278. [CrossRef]
11. Yang, D.; Xing, B.; Li, J.; Wang, Y.; Hu, N.; Jiang, S. Experiment and simulation analysis of the suspension behavior of large (5–30 mm) nonspherical particles in vertical pneumatic conveying. *Powder Technol.* **2019**, *354*, 442–455. [CrossRef]
12. Xu, H.; Zhou, J.; Ma, C.; Zhou, Z.; Liu, D.; Zhang, M. Experimental study on agglomeration characteristics and suspension velocity of cohesive adsorbent powders in a conical airflow cylinder. *Powder Technol.* **2022**, *408*, 117722. [CrossRef]
13. Hao, B.; Tong, X.; Chen, Z.; Liu, H. Calibration of simulation parameters for wind erosion gas-solid two-phase flow in arid and semiarid soils. *Rev. Bras. Eng. Agrícola Ambient.* **2022**, *26*, 564–570. [CrossRef]
14. Ren, J.; Zhou, L.; Han, L.; Zhou, J.; Yan, M. Discrete Simulation of Vertical Screw Conveyor Based on Particle Scaling Theory. *Chin. J. Process Eng.* **2017**, *17*, 936–943.

15. Jiejie, X.; Rui, Z.; Peng, W.; Xirui, Z.; Xuehu, D.; Ying, C.; Shaofeng, R. Parameter calibration of discrete element simulation model for latosol particles in hot areas of Hainan Province. *Trans. Chin. Soc. Agric. Eng.* **2020**, *36*, 158–166.
16. Guoming, H. *Discrete Element Method Analysis and Simulation of Particle System—Introduction to Industrial Application of Discrete Element Method and EDEM Software*; Wuhan University of Technology Press: Wuhan, China, 2010.
17. Nianzu, D.; Zhanfeng, H.; Yi, Q.; Xiwen, Z. Calibration and experiment of discrete element simulation parameters of red clover seeds. *J. Hebei Agric. Univ.* **2021**, *44*, 92–98.
18. Ma, X.; Hou, Z.; Liu, M. Calibration of Simulation Parameters of Coated Particles and Analysis of Experimental Results. *INMATEH Agric. Eng.* **2022**, *20*, 233–242. [CrossRef]
19. Thakur, S.C.; Ooi, J.Y.; Ahmadian, H. Scaling of discrete element model parameters for cohesionless and cohesive solid. *Powder Technol.* **2016**, *293*, 130–137. [CrossRef]
20. Tamás, K. The role of bond and damping in the discrete element model of soil-sweep interaction. *Biosyst. Eng.* **2018**, *169*, 57–70. [CrossRef]
21. Lijun, W.; Yang, L.; Chang, L.; Jiqing, M.; Wenxiu, Z. Motion Law of Maize Mixture in Cross Air-and-screen Cleaning Device. *Trans. Chin. Soc. Agric. Mach.* **2015**, *46*, 122–127.
22. Zhuo, C.; Tong, X.; Hao, B.; Chen, Z.; Liu, H. Feasibility analysis using a porous media model to simulate the wind protection effect of windbreak forests. *Land Degrad. Dev.* **2022**, *33*, 1–14. [CrossRef]
23. Lei, Z.; Xuedong, M.; Bingjiang, G.; He, D. Numerical simulation and experiment of rice cleaning. *J. Chin. Agric. Mech.* **2020**, *41*, 73–79.
24. Manfei, Z. The Sorting Properties of Alfalfa Seed and the Optimizing Design of the Control System of the Sorting Machinery. Master's Thesis, China Agricultural University, Beijing, China, 2015.
25. Yanjun, L. Flow Field Analysis and Structural Parameter Optimization of Harvesting Device of Alfalfa Seed Harvester. Ph.D. Thesis, Chinese Academy of Agricultural Mechanization Sciences, Beijing, China, 2017.
26. Gao, W.; Liu, L.; Liao, Z.; Chen, S.; Zang, M.; Tan, Y. Discrete element analysis of the particle mixing performance in a ribbon mixer with a double U-shaped vessel. *Granul. Matter* **2019**, *21*, 12. [CrossRef]